25th ABCM International Congress of Mechanical Engineering
October 20-25, 2019, Uberlândia, MG, Brazil

COB-2019-0525
ANALYSIS OF WAVE OVERTOPPING ON AN IMPERMEABLE COASTAL STRUCTURE USING A RANS-VOF NUMERICAL MODEL

Gabriela Carré dos Santos
Paulo Roberto de Freitas Teixeira
Universidade Federal do Rio Grande (FURG)
Campus Carreiros, CEP 96201-900, Rio Grande, Rio Grande do Sul, Brasil
gabrielacarre.s@gmail.com
prfreitasteixeira@gmail.com

Eric Didier
Laboratório Nacional de Engenharia Civil, Departamento de Hidráulica e Ambiente
Av. do Brasil, 101, 1700-066 Lisboa, Portugal
edidier@lnec.pt

Abstract. *The global warming is responsible for increasing the sea level and, consequently, can cause overtopping on coastal structures. The prediction of this phenomenon is difficult because involves turbulence, wave breaking and run-up. The objective of this study is to analyze numerically the wave overtopping on coastal structures by using the FLUENT® numerical model, which is based on Reynolds-Averaged Navier-Stokes equations (RANS) and uses the Volume of Fluid method (VoF) to track the interface between water and air. Influences of mesh size, turbulence model (k-ε and k-ω SST) and bottom condition (slip and no-slip) are investigated in a flume with an impermeable breakwater at its end. Two cases with different heights of incident regular waves are tested. In general, the free surface elevations up to the breakwater obtained by different conditions are very similar for both incident waves. However, the overtopping volumes have shown more important differences.*

Keywords: *breakwater, overtopping, wave-structure interaction, CFD simulation, RANS-VoF*

1. INTRODUCTION

The global warming is an important phenomenon which promotes climate changes and influences on the sea level that can cause coastal structure overtopping and, consequently, inundation and material and human risks. The project named PROTOCOL – Protección de frentes urbanos costeiros frente al calentamiento global (2019) have been developed by several institutions of different countries and it aims to analyze numerically and experimentally the influence of the sea level on overtopping of coastal structures. Novel methodologies and technical recommendations related to the coastal structure design, construction, and planning of protection of urban coastal zones will be carried out. In this project, some numerical models with different methodologies will be calibrated and validated in cases of overtopping in coastal structures.

Nowadays, there are difficulties to investigate these type of problems, since complex phenomena are involved, such as wave breaking, turbulence, run-up and overtopping. In last decades, numerical models have had important developments to deal with wave-structure interaction, but methodologies still must be improved to reach a good accuracy with a low computational time consuming mainly in cases which occur overtopping on coastal structures. In this study, the FLUENT® numerical model (FLUENT, 2016), which is based on Reynolds-Averaged Navier-Stokes (RANS) equations and uses the VoF method to track the free surface, is used to simulate the overtopping flow due to the interaction between an incident regular wave and an impermeable coastal structure. The influence of some important numerical conditions is analyzed; more specifically, the sensibility analysis is performed for the mesh resolution, the bottom boundary condition (slip and no-slip) and the turbulence model (k-ε and k-ω *SST*). Therefore, results in terms of free surface elevations and overtopping volumes are analyzed to quantify the influence of each condition on the behavior of the interaction between waves and the coastal structure.

2. NUMERICAL MODEL

RANS-VoF equations, based on the decomposition of the instantaneous velocity and pressure fields of the Navier–Stokes equations into mean and fluctuating components, and the subsequent time-averaging of the set of equations, are

used. This process introduces Reynolds stress terms associated with the turbulence. Two turbulence models are used for relating Reynolds stresses to mean flow variables and close the equations: the standard k-ε turbulence model and the k-ϖ *SST* turbulence model, both with standard parameters.

Free surface flow motion is defined by the VoF method (Hirt and Nichols, 1981), which is based on the transport equation of the volume fraction, a scalar that takes values 0 in the air, 1 in the water and 0.5 at the free surface.

The RANS-VoF numerical model FLUENT® (FLUENT, 2016) is employed and applies a Finite Volume technique to solve RANS and VoF equations, where variables are defined in the center of each control volume.

In the FLUENT® numerical model, the solver scheme SIMPLEC (with standard under-relaxation factors) and the scheme PRESTO! are used for discretizing pressure. The momentum is discretized by the third-order scheme MUSCL, and the turbulence kinetic energy and dissipation rate are discretized by the second order upwind scheme. Geo-reconstruct scheme (FLUENT, 2016), well adapted for modeling complex shape of free surface flow, like wave breaking and overtopping, is used for the VoF equation, compatible with the first order time integration scheme and variable time step.

3. CASE STUDY

The study case consists of a small flume at 0.25 m depth with a wave maker and an impermeable breakwater at its end, which has a similar geometry to that of the Albufeira harbour at the south of Portugal at 1:30 scale (Fig. 1) (Didier et al., 2013). From the wave maker to the toe of the breakwater, the flume has a ramp 2.5% slope and 2 m long. The breakwater 0.75 m long has a slope of 7.5:3.

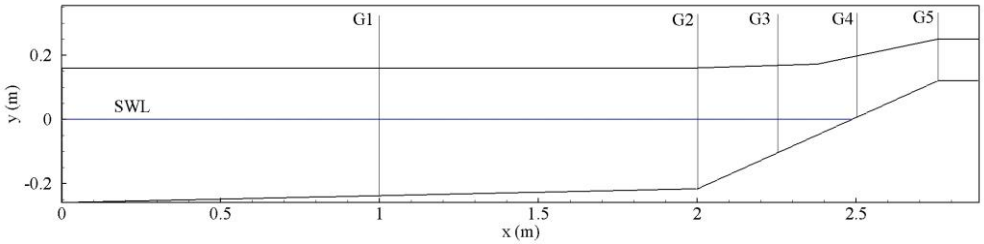

Figure 1. Computational domain with gauges position: G1 and G2 inside the wave flume, G3 and G4 on the breakwater and G5 at the beginning of the breakwater crest

Two cases of incident regular waves are considered, both with a wave period $T = 2.1909$ s and wave height $H = 0.0506$ m and 0.0806 m. Free surface elevations are measured by five gauges along the domain (Fig. 1): gauges G1 and G2 inside the flume before the breakwater; G3 and G4 at the slope zone; and G5 at beginning of the breakwater crest. Overtopping volume is calculated at gauge G5 using the overtopping discharge measured along the simulation. Overtopping occurs for both configurations and wave breaking is spilling type.

The incident wave is generated at the wave maker boundary, imposing velocity component profiles and the correspondent free surface elevation of the linear wave theory (Dean and Dalrymple, 2000) by means of UDF (User Define Function) (FLUENT, 2016). Additionally, an active absorption method (Didier and Neves, 2012; Didier et al., 2017; Teixeira et al., 2017) is employed at the wave maker boundary to eliminate the reflected wave from the coastal structure.

Atmospheric pressure is imposed on the top boundary of the flume. At the end of the flume, on the breakwater crest, an exit boundary condition allows the water discharge flows out from the computational domain. Two types of boundary condition, imposed on the bottom of the flume and the coastal structure, are tested: a non-slip and a slip condition, which allows analyzing more specifically the effect of friction on the wall. Furthermore, two turbulence models are tested, standard k-ε and k-ω *SST* both with standard parameters.

Four regular meshes using quadrilateral cells are constructed varying the horizontal, *dx*, and vertical, *dy*, resolution. Mesh resolution for wave propagation was already defined by previous studies (Teixeira et al., 2013; Mendonça et al., 2018) recommending 70 cells per wavelength and 20 cells for wave height. So that only resolution in the vicinity of the coastal structure, i.e. on the slope and the crest of the breakwater, where wave breaking and overtopping occur, was refined to perform a resolution convergence analysis of overtopping discharge. Control volume number varies from 19380 to 49950 for meshes M0 and M3, respectively, depending essentially of *dx* and *dy* resolution in the vicinity of the coastal structure (Table 1). Figure 2 shows the coarser mesh M0.

As referred before, a variable time step is used for time integration. The courant number is 0.7 and time step is limited between $3.0\text{x}10^{-3}$ s and $0.155\text{x}10^{-3}$ s. The maximum time step, $3.0\text{x}10^{-3}$ s, which corresponds approximately to $T/600$, is defined from previous studies using implicit formulation and second order scheme for time integration (Didier et al., 2011; Paixão Conde et al., 2011; Teixeira et al., 2013). The minimum time step is around 20 times smaller than the maximum time step which is enough to resolve correctly the set of equation at each time step since the wave

breaking is spilling type. For a plugging wave breaking, the minimum time step would be smaller. Finally, six non-linear iterations per time step enable to reduce the residue by at least two orders of magnitude which are enough for good accuracy (Didier et al., 2011; Paixão Conde et al., 2011; Teixeira et al., 2013).

Table 1. Mesh resolutions

Mesh	Number of elements	*dx* (x10^{-2} m)	*dy* (x10^{-2} m)
M0	19380	1.1	0.28
M1	21090	1.1	0.08
M2	33510	0.4	0.08
M3	49950	0.2	0.04

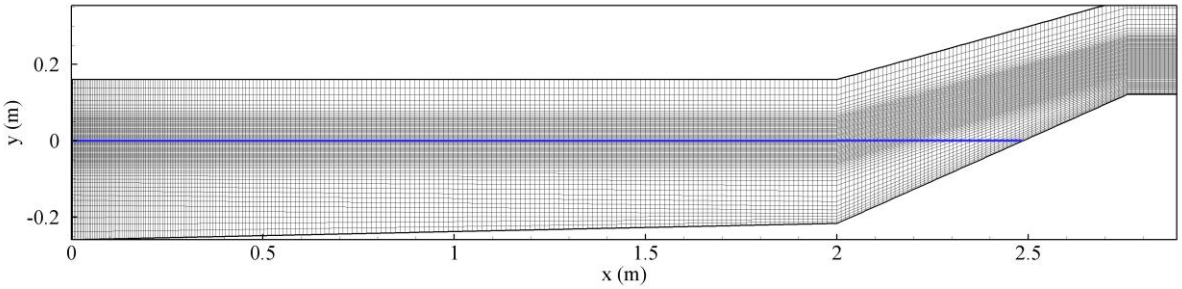

Figure 2. Mesh M0 of the computational domain: blue line indicates the still water level

4. RESULTS AND DISCUSSION

The influence of some important numerical conditions is analyzed; more specifically, the sensibility analysis is performed for mesh resolution, the bottom boundary condition (no-slip and slip) and the turbulence model (k-ε and k-ω *SST*). Therefore, results in terms of free surface elevations, η, overtopping volumes, Q, and overtopping discharge, Qt, are analyzed to quantify the influence of each condition on the behavior of the interaction between incident waves and the breakwater.

Time series of free surface elevation are presented at some gauges along the wave flume and at the breakwater crest, gauge G5, where overtopping volume is calculated from the monitored overtopping discharge. The volume overtopping is analyzed for the 1st wave overtopping which allows evaluating only the influence of interaction between the incident wave and the breakwater on the overtopping. The total overtopping volume is also analyzed at the 5th and 12th wave overtopping which allows evaluating the influence of interaction between incident wave, breakwater and reflected wave. Analysis of overtopping discharge is also performed from the 5th to 12th wave overtopping which corresponds to the periodic wave-structure interaction after transitional flow.

Analyses of *rmse* (root-mean-square) and *IC* (index of agreement) (Willmott et al., 1985) are also performed for the complete time series of free surface elevation for the time interval from 0.0 to 30.0 s (end of simulations).

4.1 Mesh resolution analysis

Sensibility of results with mesh resolution is performed using no-slip boundary condition at walls and turbulence model k-ε. Figures 3 and 4 shows temporal series of the free surface elevation at gauge G1 and G2 and free surface elevation and overtopping volume at gauge G5 for meshes M0 to M3 for incident wave H = 0.0506 and 0.0806 m, respectively. Table 2 presents the *rmse* and *IC* indices for time series of free surface elevation at gauges G1 to G5 for H=0.0506 and 0.0806 m, comparing results obtained for mesh M0, M1 and M2 with results obtained for mesh M3. Table 3 presents the overtopping volume, Q, at wave overtopping 1, 5 and 12 and overtopping discharge, Qt, calculated from waves 5 to 12, for H= 0.0506 and 0.0806 m, and the relative differences of ΔQ and ΔQt comparing results obtained for mesh M0, M1 and M2 with results obtained for mesh M3.

Overtopping occurs for both incident wave heights (Fig. 3(c), (d) and 4(c), (d)) but overtopping volume is around 20 times smaller for H = 0.0506 m than H = 0.0806 m at the end of the simulation, with Q = 3.79 x10^{-3} and 60.64 x10^{-3} m^3/m, respectively (Tab. 3).

Free surface elevations at gauges G1 to G2 for both wave heights (Fig. 3(a) and (b) and Fig. 4(a) and (b)) are not significantly affected by the mesh resolution with only small differences. This is confirmed by *rmse* and *IC* indices values in Tab. 2: *rmse* values have the same order of magnitude, globally smaller than 1.0x10^{-3} m and between 0.5 to 1.0x10^{-3} m for both wave heights; and *IC* values are globally larger than 0.999 for both wave heights, excepted for gauge G5 that presents smaller *IC*, which is smaller for H = 0.0506 m than H = 0.0806 m. For all gauges and both

incident wave heights, convergence with mesh resolution is observed for *rmse* and *IC* indices: the *rmse* values decreases with mesh refinement and *IC* increases.

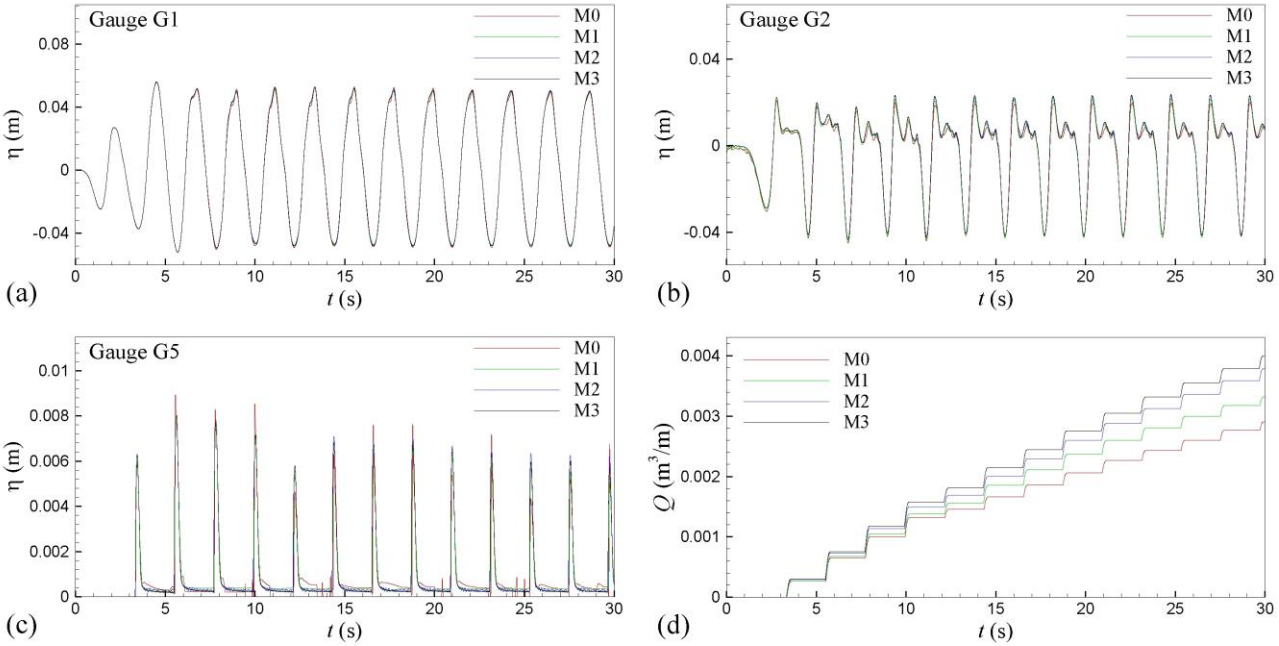

Figure 3. Free surface elevation at gauges (a) G1, (b) G2 and (c) G5 and (d) overtopping volume at gauge G5 for meshes M0 to M3 for H=0.0506m, k-ε turbulence model and no-slip boundary condition at walls

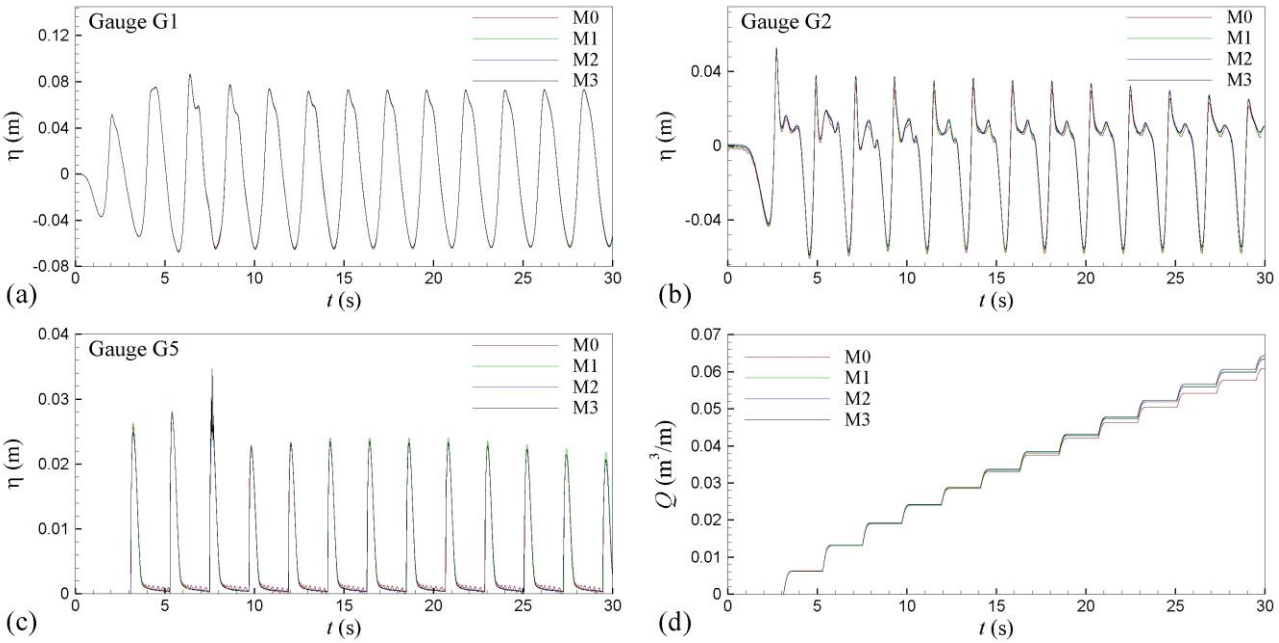

Figure 4. Free surface elevation at gauges (a) G1, (b) G2 and (c) G5 and (d) overtopping volume at gauge G5 for meshes M0 to M3 for H=0.0806m, k-ε turbulence model and no-slip boundary condition at walls

Overtopping shows more sensibility to mesh resolution (Fig. 3(c) and (d) and Fig. 4(c) and (d)) than free surface elevation. Overtopping discharge is smaller for incident wave H = 0.0506 m than H = 0.0806 m and so that overtopping discharge is more mesh resolution dependent. Convergence is obtained for incident wave H = 0.0806 m (Fig. 4(d)), but it is not so clear for H = 0.0506 m, even if a convergence tendency is observed (Fig. 3(d)). Table 3 confirmed the previous observations and allows a deeper analysis. The first wave overtopping, which characterizes the wave-structure interaction, shows a good convergence of overtopping volume with mesh refinement, with differences between mesh M2 and M3 of 0.010×10^{-3} and 0.017×10^{-3} m^3/m, i.e. a relative difference of 3.47 and 0.28% for incident wave height 0.0506 m and 0.0806 m, respectively. Comparison of overtopping volume at overtopping wave 5 and 12, which allows to verify the wave-structure and incident-reflected wave interactions, shows larger differences than first wave

overtopping. However, it can be seen that convergences with mesh refinement is confirmed: differences for the overtopping volume of the 12th wave are 0.195 and 0.889 x10^{-3} m^3/m between mesh M2 and M3, i.e. a relative difference of 5.15 and 1.47% for incident wave height 0.0506 m and 0.0806m, respectively. Finally, the overtopping discharge *Qt* calculated between the 5th and 12th wave, which corresponds to a periodic wave-structure interaction, shows very good convergence with mesh refinement since the relative difference between mesh M2 and M3 is only 3.65 and 2.75% for incident wave height 0.0506 m and 0.0806 m, respectively.

Table 2. *rmse* and *IC* indices for free surface elevation at gauges G1 to G5 for H=0.0506 and 0.0806 m, k-ε turbulence model and no-slip boundary condition at walls (comparison between meshes M0, M1 and M2 with mesh M3)

H=0.0506 m	*rmse* (x10^{-3} m)					*IC*				
Gauge	1	2	3	4	5	1	2	3	4	5
M0	0.646	1.294	1.278	0.661	0.570	0.9999	0.9987	0.9996	0.9998	0.9693
M1	0.473	0.688	1.045	0.554	0.506	1.0000	0.9996	0.9997	0.9999	0.9774
M2	0.475	0.649	0.803	0.505	0.463	1.0000	0.9997	0.9998	0.9999	0.9808

H=0.0806 m	*rmse* (x10^{-3} m)					*IC*				
Gauge	1	2	3	4	5	1	2	3	4	5
M0	0.825	2.265	1.788	0.886	0.759	0.9999	0.9979	0.9996	0.9998	0.9973
M1	0.548	0.773	1.523	0.769	0.606	1.0000	0.9998	0.9997	0.9998	0.9983
M2	0.335	0.794	1.259	0.584	0.471	1.0000	0.9997	0.9998	0.9999	0.9989

Table 3. Overtopping volume at wave overtopping 1, 5 and 12 and overtopping discharge between the 5th and 12th wave for H=0.0506 and 0.0806 m, k-ε turbulence model and no-slip boundary condition at walls

H=0.0506 m	Overtopping volume Q (x10^{-3} m^3/m)			Qt (x10^{-1} m^3/s/m)	Differences of overtopping volume ΔQ (%)			ΔQt (%)
Overtopping	1	5	12	5 to 12	1	5	12	5 to 12
M0	0.261	1.460	2.769	0.853	13.00	19.47	26.89	33.69
M1	0.266	1.561	3.176	1.053	11.47	13.91	16.13	18.18
M2	0.290	1.690	3.592	1.240	3.47	6.79	5.15	3.65
M3	0.300	1.813	3.787	1.287	-	-	-	-

H=0.0806 m	Overtopping volume Q (x10^{-3} m^3/m)			Qt (x10^{-1} m^3/s/m)	Differences of overtopping volume ΔQ (%)			ΔQt (%)
Overtopping	1	5	12	5 to 12	1	5	12	5 to 12
M0	6.237	28.441	57.685	19.069	0.67	1.32	4.87	8.08
M1	6.173	28.565	59.957	20.469	0.36	0.89	1.12	1.33
M2	6.212	28.806	59.746	20.174	0.28	0.05	1.47	2.75
M3	6.195	28.822	60.635	20.744	-	-	-	-

4.2 No-slip and slip boundary condition at walls

Results obtained by two wall boundary conditions, no-slip and slip, are compared using k-ε turbulence model and mesh M2. Figures 5 and 6 show temporal series of the free surface elevation at gauge G1 and overtopping volume at gauge G5 for incident wave H = 0.0506 m and 0.8060 m, respectively. Table 4 presents *rmse* and *IC* indices at gauges G1 to G5, comparing the time series of free surface elevation obtained on both wall boundary conditions. Table 5 shows the overtopping volume, Q, at wave overtopping 1, 5 and 12 and overtopping discharge, Qt, between the 5th and 12th wave for both wall boundary conditions and the relative differences ΔQ and ΔQt.

Slip boundary condition at walls induces an increase of overtopping volume for both incident wave heights (Fig. 5(b) and Fig. 6(b)). Nevertheless, free surface elevation is not significantly modified, as it can be seen in Fig. 5(a) and Fig. 6(a) at gauge G1. This is confirmed in Tab. 4 by *rmse* and *IC* indices at gauge G1 to G5: *rmse* is around 1.0x10^{-3} m for both wave heights and *IC* values are globally around 0.999 or slightly smaller.

Overtopping volume shows some differences due to the type of wall boundary condition (Tab. 5). The first wave overtopping shows a volume difference, between both wall boundary conditions, of 0.048 and 0.258x10^{-3} m^3/m, i.e. a relative difference of 14.2 and 3.99% for incident wave height 0.0506 m and 0.0806 m, respectively. Comparison of overtopping volume at the 12th overtopping wave shows the same order of differences than first wave overtopping: differences are 0.453 and 1.754x10^{-3} m^3/m, between both wall boundary conditions, i.e. a relative difference of 11.2 and 2.95% for incident wave height 0.0506 m and 0.0806m, respectively. The overtopping discharge Qt calculated between

the 5th and 12th wave presents a discharge difference of 0.067 and 0.447x10^{-1} m^3/s/m, between both wall boundary conditions, which corresponds to a relative difference of 5.13 and 2.17%.

Table 6 presents the mean of maximum water height of waves overtopping at gauge G5 and the mean overtopping volume per wave between the 5th and 12th wave overtopping. As observed before for the overtopping volume and discharge, the mean overtopping per wave increases using slip boundary condition at walls for both incident wave heights. However, for incident wave height 0.0506 m, mean of maximum water height at gauge G5 decreases 10.06% comparing no-slip and slip boundary condition, whereas mean overtopping per wave increases 7.66% which seems indicating that velocity increases on the breakwater. For incident wave 0.0806 m, mean of maximum water height at gauge G5 increases 6.77%, whereas mean overtopping per wave increases only 2.37%.

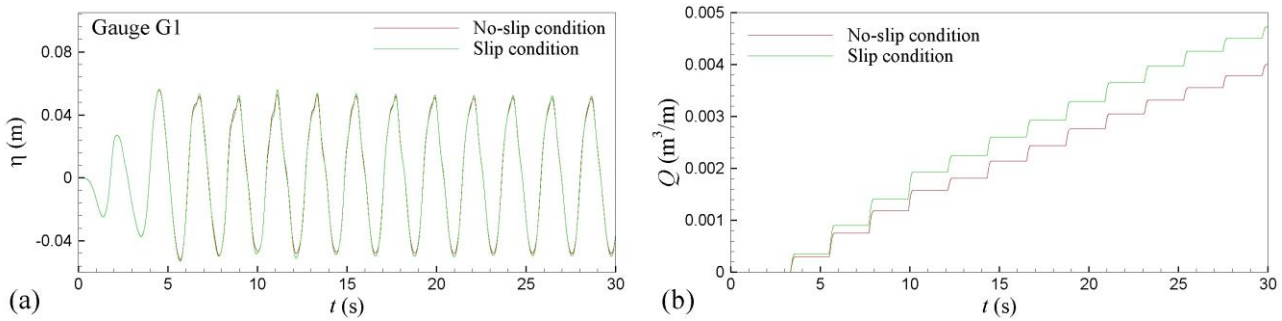

Figure 5. Free surface elevations at (a) gauges G1 and (b) overtopping volume at gauge G5 for mesh M2 and H = 0.0506 m, k-ε turbulence model and no-slip and slip boundary condition at walls

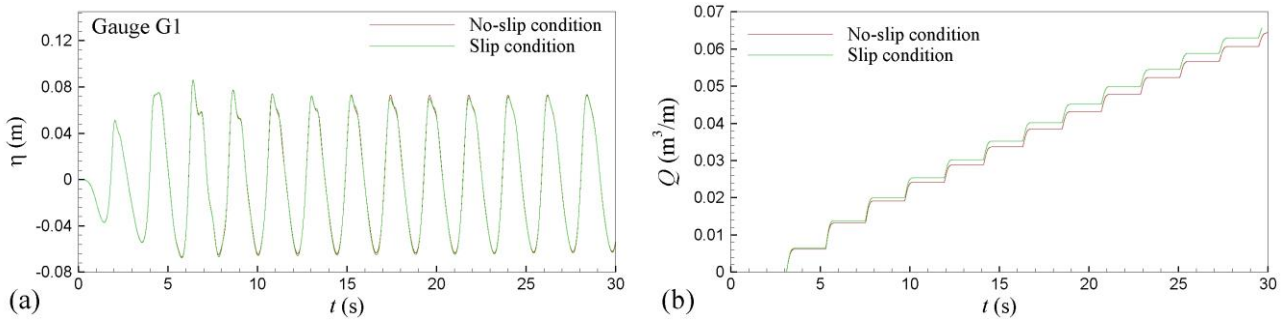

Figure 6. Free surface elevations at (a) gauges G1 and (b) overtopping volume at gauge G5 for mesh M2 and H = 0.0806 m, k-ε turbulence model and no-slip and slip boundary condition at walls

Table 4. *rmse* and *IC* indices for free surface elevations at gauges G1 to G5 for H = 0.0506 m and 0.0806 m, k-ε turbulence model and mesh M2 (comparison between no-slip and slip boundary condition at walls)

	rmse (x10^{-3} m)					*IC*				
Gauge	1	2	3	4	5	1	2	3	4	5
H=0.0506 m	1.260	1.946	2.542	0.598	0.275	0.9997	0.9971	0.9984	0.9998	0.9931
H=0.0806 m	1.053	2.241	2.189	1.002	0.396	0.9999	0.9979	0.9994	0.9997	0.9992

Table 5. Overtopping volume at wave overtopping 1, 5 and 12 and overtopping discharge between the 5th and 12th wave for H = 0.0506 m and 0.0806 m, k-ε turbulence model, mesh M2 and no-slip and slip boundary condition at walls

	Wall boundary condition	Overtopping volume Q (x10^{-3} m^3/m)			Qt (x10^{-1} m^3/s/m)	Difference of overtopping volume ΔQ (%)			ΔQt (%)
		1	5	12	5 to 12	1	5	12	5 to 12
H=0.0506 m	No-slip	0.290	1.690	3.592	1.240	-	-	-	-
	Slip	0.338	2.041	4.045	1.307	14.20	17.20	11.20	5.13
H=0.0806 m	No-slip	6.212	28.806	59.746	20.174	-	-	-	-
	Slip	6.470	29.935	61.560	20.621	3.99	3.77	2.95	2.17

Table 6. Mean of maximum water height at gauge G5 and mean overtopping volume per wave for H = 0.0506 and 0.0806 m, k-ε and no-slip or slip boundary condition at walls

	Turbulence model	Wall boundary condition	Mean of maximum water height at G5 (x10^{-2} m)	Mean overtopping volume per wave (x10^{-3} m^3/m)
H=0.0506 m	k-ε	no-slip	0.659	0.261
	k-ε	slip	0.599	0.283
H=0.0806 m	k-ε	no-slip	2.235	4.441
	k-ε	slip	2.398	4.549

4.3 Turbulence model: k-ε and k-ϖ *SST*

Results obtained by two turbulence models, k-ε and k-ϖ *SST*, are compared using slip boundary condition at walls and mesh M2. Figures 7 and 8 show temporal series of the free surface elevation at gauge G1 and overtopping volume at gauge G5 for incident wave H=0.0506 m and 0.8060 m, respectively. Table 7 presents *rmse* and *IC* indices at gauges G1 to G5, comparing time series of the free surface elevation obtained in both turbulence models. Table 8 shows the overtopping volume, Q, at wave overtopping 1, 5 and 12 and overtopping discharge, Qt, between the 5th and 12th wave and the relative differences ΔQ and ΔQt.

Using k-ϖ *SST* turbulence model induces an increase of overtopping volume for both incident wave heights as observed in Fig. 7(b) and Fig. 8(b).

Free surface elevation is not significantly modified, as shown in Fig. 7(a) and Fig. 8(a) for gauge G1. However, it can be noted in Tab. 7 that *rmse* at gauge G1 to G5 is smaller for incident wave height 0.0506 m, with values between 0.201 and 1.611 m, than for incident wave height 0.0806 m, with values between 0.957 and 4.089 m. *IC* is larger than 0.999 for both wave heights at gauge G1. For the smallest wave height, *IC* is larger than 0.999 at gauge G2 to G4. However, for wave height 0.0806 m, *IC* is smaller than 0.999 at gauge G2 to G4. At gauge G5, *IC* is similar for both wave heights, around 0.996. These results show that the turbulence model modifies significantly the flow. It also seems that the influence of the turbulence model is more important for the largest wave height which is associated to larger velocity magnitude in the wave propagation and run-up/run-down on the breakwater.

The first wave overtopping shows very similar overtopping volume for both incident wave heights and turbulence models with an absolute difference of 0.001 and 0.126x10^{-3} m^3/m between both turbulence models, i.e. a relative difference of 0.29 and 1.91%, for incident wave height 0.0506 m and 0.0806 m, respectively (Tab. 8). Comparison of overtopping volume at the 12th overtopping wave shows that differences are 0.325 and 3.390x10^{-3} m^3/m between the both turbulence models, i.e. a relative difference of 7.44 and 5.22% for incident wave height 0.0506 and 0.0806m, respectively. The overtopping discharge Qt calculated between the 5th and 12th wave presents a discharge difference of 0.146 and 2.092x10^{-1} m^3/s/m between both turbulence models which corresponds to a relative difference of 10.05 and 9.21%.

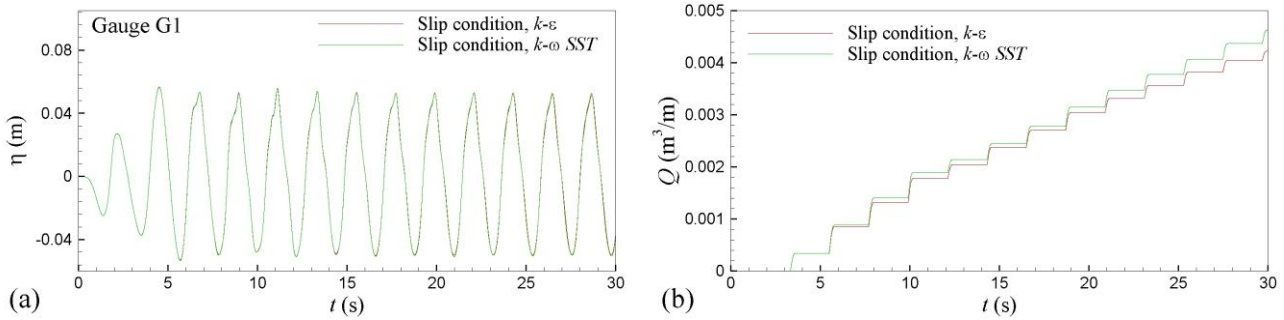

Figure 7. Free surface elevation at (a) gauges G1 and (b) overtopping volume at gauge G5 for mesh M2 and H=0.0506m, slip boundary condition at walls and k-ε and k-ϖ *SST* turbulence model

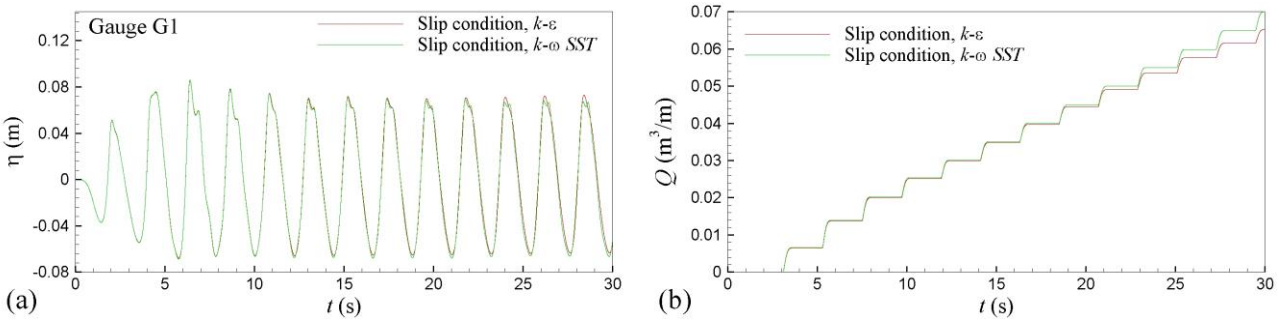

Figure 8. Free surface elevation at (a) gauges G1 and (b) overtopping volume at gauge G5 for mesh M2 and H=0.0806m, slip boundary condition at walls and k-ε and k-ϖ *SST* turbulence model

Table 7. *rmse* and *IC* indices for free surface elevations at gauges G1 to G5 for H=0.0506 and 0.0806 m, mesh M2 and slip boundary condition at walls (comparison between k-ε and k-ϖ *SST* turbulence model)

	rmse (x10^{-3} m)					*IC*				
Gauge	1	2	3	4	5	1	2	3	4	5
H=0.0506 m	0.789	0.880	1.611	0.360	0.201	0.9999	0.9995	0.9994	0.9999	0.9964
H=0.0806 m	2.623	4.089	3.319	2.383	0.957	0.9993	0.9937	0.9985	0.9984	0.9959

Table 8. Overtopping volume at wave overtopping 1, 5 and 12 and overtopping discharge between the 5th and 12th wave for H=0.0506 and 0.0806 m, mesh M2, slip boundary condition at walls and k-ε and k-ϖ *SST* turbulence model

	Turbulence model	Overtopping volume Q (x10^{-3} m^3/m)			Qt (x10^{-1} m^3/s/m)	Difference of overtopping volume ΔQ (%)			ΔQt (%)
		1	5	12	5 to 12	1	5	12	5 to 12
H=0.0506 m	k-ε	0.338	2.041	4.045	1.307	-	-	-	-
	k-ϖ *SST*	0.339	2.141	4.370	1.453	0.29	4.67	7.44	10.05
H=0.0806 m	k-ε	6.470	29.935	61.560	20.621	-	-	-	-
	k-ϖ *SST*	6.596	30.116	64.950	22.713	1.91	0.60	5.22	9.21

Table 9. Mean of maximum water height at gauge G5 and mean overtopping volume per wave for H = 0.0506 m and 0.0806 m, k-ε and k-ϖ *SST* with slip boundary condition at walls

	Turbulence model	Wall boundary condition	Mean of maximum water height at G5 (x10^{-2} m)	Mean overtopping volume per wave (x10^{-3} m^3/m)
H=0.0506m	k-ε	slip	0.599	0.283
	k-ϖ *SST*	slip	0.647	0.310
H=0.0806 m	k-ε	slip	2.398	4.549
	k-ϖ *SST*	slip	2.569	4.943

Slip boundary condition at walls induces an increase of overtopping volume comparing with no-slip boundary condition for both incident wave heights. However, for incident wave height 0.0506 m, mean of maximum water height at gauge G5 decreases 10.06% comparing no-slip and slip boundary condition but mean overtopping per wave increases 7.66% which seems indicating that velocity increases on the breakwater. For incident wave 0.0806 m mean of maximum water height at gauge G5 increases 6.77% but mean overtopping per wave increases only 2.37%.

Table 9 presents the mean of maximum water height of waves overtopping at gauge G5 and the mean overtopping volume per wave between the 5th and 12th wave overtopping. Mean of maximum water height at gauge G5 increases 7.34 and 6.67% for both incident wave heights and mean overtopping per wave increases 8.54 and 7.97% for incident wave H = 0.0506 m and 0.0806 m, respectively. It can be notice that the relative increase of mean of maximum water height at gauge G5 and mean overtopping per wave are rather similar. This result seems indicating that k-ϖ *SST* turbulence model is less dissipative than k-ε.

Figure 9 shows 8 time shoots of free surface flow along a wave period at each T/8 s instants for H=0.0806 m using slip boundary condition at walls and k-ϖ *SST* turbulence model, that are numerical options which seem the more appropriated for modelling wave overtopping of impermeable breakwater. It can be seen that wave breaking is spilling type. The interaction between the incident wave and the reflected one by the breakwater is evident. The complex interaction between the flow at the toe of the breakwater and the run-down flow on the inclined breakwater wall can

also be seen. These non-linear interactions and the phase between the various involved phenomena have a determinant action on the type of wave breaking and consequently on the overtopping discharge.

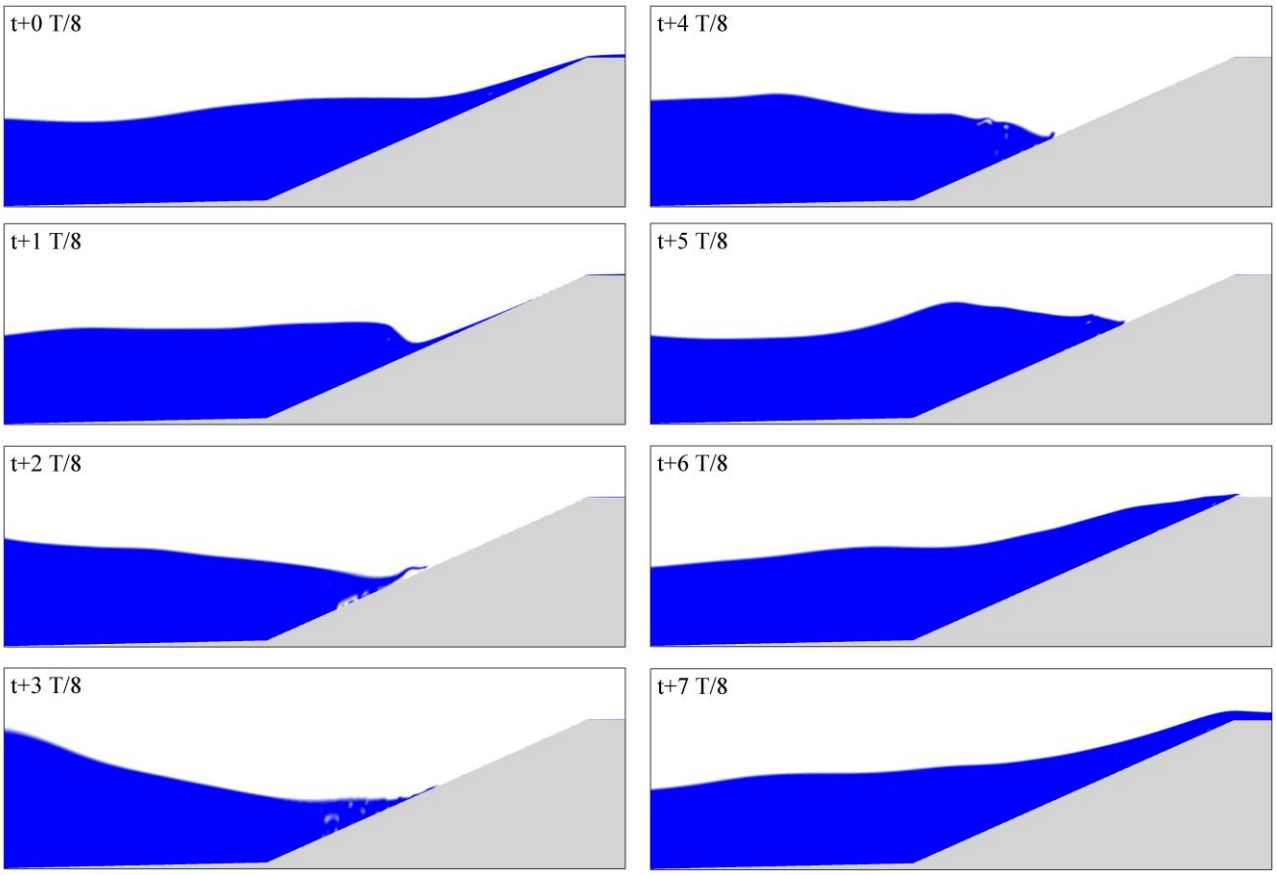

Figure 9. Free surface flow for H = 0.0806 m, mesh M2, slip boundary condition at walls and k-ϖ *SST* turbulence model at 8 instants along a wave period

5. CONCLUSIONS

FLUENT® numerical model which is based on Reynolds-Averaged Navier-Stokes equations and VoF method to model free surface flows was used to simulate the overtopping flow due to the interaction between an incident regular wave and an impermeable coastal structure. The influence of mesh resolution, boundary condition at walls (no-slip and slip) and turbulence model (k-ε and k-ϖ *SST*) on the behavior of the interaction between waves and the coastal structure is analyzed comparing free surface elevations and overtopping volume and discharge.

The study shows that overtopping is a very sensible phenomenon for modeling which depends of mesh resolution, boundary conditions at walls and turbulence model. Mesh analysis shows that convergence of overtopping volume requires a fine mesh at the breakwater walls and breakwater crest with a resolution of around 20 to 30 elements for the maximum of water height at the breakwater crest. Slip boundary condition at walls induces an increase of overtopping volume. This hypothesis is relatively consistent with impermeable breakwater without significant wall roughness. k-ϖ *SST* turbulence model seems less dissipative than k-ε which induces an increase of overtopping volume. For a same mesh resolution, k-ϖ *SST* turbulence model and slip boundary conditions at walls allow the larger overtopping discharge. This model is a consistent model that avoids excessive refined mesh at walls, a necessary condition using k-ϖ *SST* turbulence model with no-slip boundary condition at walls.

In future study, numerical results will be compared with experimental data to confirm the better options of the numerical model for modeling wave breaking and wave overtopping of impermeable breakwater.

6. ACKNOWLEDGEMENTS

This study was financed in part by the Coordenação de Aperfeiçoamento de Pessoal de Nível Superior - Brasil (CAPES) - Finance Code 001.

Eric Didier acknowledges the project PROTOCOL - Protección de frentes urbanos costeros frente al calentamiento global, CYTED 2017-PE-PROTOCOL.

7. REFERENCES

Dean, R.G. and Dalrymple, R.A., 2000. Water wave mechanics for engineers and scientists, London: World scientific publishing Co. Pte. Ltd.

Didier, E., Paixão Conde, J.M., and Teixeira, P.R.F., 2011. "Numerical simulation of an oscillation water column wave energy converter with and without damping". *In Proceedings of the VII International Conference on Computational Methods in Marine Engineering - MARINE 2011*. Lisbon, Portugal, pp. 206-217.

Didier, E. and Neves, M.G., 2012. "A semi-infinite numerical wave flume using Smoothed Particle Hydrodynamics". *International Journal of Offshore and Polar Engineering*, Vol. 22, Nº3, pp. 193-199.

Didier E., Neves D.R.C.B, Teixeira P.R.F., Neves M.G., Soares H., and Viegas M., 2013. "Coupling of FLUINCO mesh-based and SPH mesh-free numerical codes for the modelling of wave overtopping over a porous breakwater". *In Proceedings of the 6th SCACR – International Short Course/Conference on Applied Coastal Research*. Lisbon, Portugal.

Didier, E., Teixeira, P.R.F., and Neves M.G., 2017. "A 3D Numerical Wave Tank for Coastal Engineering Studies". *Defect and Diffusion Forum*, Vol. 372, pp. 1-10.

FLUENT, 2016. User's Guide, ANSYS Inc.

Hirt, C.W. and Nichols, B.D., 1981. "Volume of fluid (VOF) method for the dynamics of free boundaries". *Journal of computational physics*, Vol. 39, pp. 201-225.

Mendonça, A., Dias, J., Didier, E., Fortes, C.J.E.M., Neves, M.G. Reis, M.T., Conde, J.M.P., Poseiro, P., and Teixeira, P.R.F., 2018. "An integrated tool for modelling oscillating water column (OWC) wave energy converters (WEC) in vertical breakwaters". *Journal of Hydro-environment Research*, vol. 19, pp.198-213.

Paixão Conde, J.M., Teixeira, P.R.F., and Didier, E., 2011. "Numerical simulation of an oscillating water column wave energy converter: Comparison of two numerical codes". *In Proceedings of the 21th International Offshore and Polar Engineering Conference*. Maui, USA, pp. 688-674

PROTOCOL, 2019. "PROTOCOL – Protección de frentes urbanos costeiros frente al calientamiento global" 22. Mar. 2019 <https://gdfa.ugr.es/protocol>.

Teixeira P. R. F., Davyt, D. P., Didier, E., and Ramalhais, R., 2013. "Numerical simulation of an oscillating water column device using a code based on Navier Stokes equations". *Energy*, vol. 61, Nº1, pp. 513–530.

Teixeira, P.R.F., Didier, E., and Neves, M.G., 2017. "A 3D RANS-VOF wave tank for oscillating water column device studies". *In Proceedings of the MARINE*. Nantes, France, pp. 710-721.

Willmott, C.J., Ackleson, S.G., Davis, R.E., Feddema, J.J., Klink, K.M., Legates, D.R., O'Donnell, J., and Rowe, C.M., 1985. "Statistics for the evaluation and comparison of models". *J. Geophys. Res.*, vol. 90(c5), pp. 8995–9005.

8. RESPONSIBILITY NOTICE

The authors are the only responsible for the printed material included in this paper.